2026 IEEE International Conference on Robotics and Automation (ICRA 2026)
June 1-5, 2026. Vienna, Austria

A Lightweight Hip Exoskeleton with High Torque-to-Mass Ratio: Design, Gait-Synchronized Control, and Physiological Validation

Tzy-Qian Pai, Shi-Mou Lin, and Chao-Chieh Lan, *Senior Member*, *IEEE*

***Abstract*—This paper presents the design, control, and experimental validation of a lightweight hip exoskeleton for walking assistance. By integrating quasi-direct drive actuators, single-piece stainless steel frames, and passive revolute joints, the device achieves a high torque-to-mass ratio while maintaining a compact and lightweight structure. A delayed output feedback control strategy synchronizes assistive torque with the gait cycle by actively leading the wearer's hip motion, with user studies identifying a consistent optimal phase difference across participants and walking speeds, eliminating repeated calibration. Surface electromyography validates the assistance, demonstrating substantial reductions in activation of the vastus medialis and vastus lateralis at the optimal time delay. Power analysis further confirms that this setting maximizes positive power transfer while minimizing resistive effects. The proposed exoskeleton delivers physiologically meaningful and energetically efficient hip assistance suitable for everyday mobility support.**

***Index Terms*—Hip exoskeleton robot, direct-drive actuator, torque-to-mass ratio, passive joint, surface electromyography, gait cycle, optimal assistance.**

I. INTRODUCTION

Mobility impairments arising from age-related muscle decline, neurological disorders, or degenerative diseases are increasingly prevalent as global populations age, reducing independence and raising the risk of falls. Wearable exoskeleton robots [1-4] offer a promising means of mechanical assistance, yet practical adoption remains limited by excessive device weight, short battery life, complex control requirements, and discomfort during prolonged use. Achieving a system that is simultaneously lightweight, comfortable, and adaptable across diverse walking conditions remains an open challenge.

Among wearable assistive devices, hip exoskeletons have received particular attention given the hip joint's dominant contribution to locomotion power generation. The choice of actuation technology fundamentally shapes a hip exoskeleton's performance characteristics. Quasi-direct drive actuators [5-6] achieve high backdrivability and responsive torque control, but their low gear ratios typically yield unfavorable torque-to-mass ratios, necessitating larger and heavier motors. SEA-based designs [7-9] introduce mechanical compliance between the motor and load, enabling accurate torque estimation and improved human-robot interaction, at the cost of added weight, mechanical complexity, and reduced bandwidth. Bowden cable transmissions [10-11] decouple the motor from the joint by routing cables remotely, alleviating limb-worn mass, but introduce frictional losses and compliance variability that can compromise force transmission fidelity.

The mechanical structure of hip exoskeletons also significantly influences performance, comfort, and user acceptance. Conventional designs employ rigid frameworks with adjustable linkages [9], requiring a careful balance between rigidity and weight. Recent designs have incorporated lightweight materials such as carbon fiber [12-13] and stainless steel, while passive joints [5-6, 8-9] are commonly integrated to compensate for misalignment between the device and human joints, improving comfort and reducing stress.

Surface electromyography (sEMG) has been widely recognized as a reliable indicator of muscle activation, providing a direct measurement of neuromuscular effort during movement [14-15]. Using sEMG allows for quantifying how much muscle demand decreases when wearing an exoskeleton, making it a key tool to assess assistive performance. Although sEMG can serve as a human-in-the-loop control signal to optimize assistance, attaching sEMG sensors during daily walking is impractical. It is important to develop an optimal control strategy based on sEMG experiments that can be applied across different users and walking speeds, ensuring the assistance provided is both mechanically efficient and physiologically meaningful.

Building on these insights, this paper considers a lightweight hip exoskeleton employing direct-drive actuators. Based on our earlier work [16], which presented the mechanical design and structural analysis of this hip exoskeleton, this paper further develops the torque control strategy and provides comprehensive physiological validation through sEMG experiments and power analysis. Sec. 2 of this paper details the proposed lightweight hip exoskeleton design, followed by a torque control strategy for the exoskeleton in Sec. 3. In Sec. 4, experiments are conducted to evaluate the optimal assistance based on user feedback. The optimal assistance parameters are then verified by the surface electromyography experiments in Sec. 5 and power analysis in Sec. 6. Finally, conclusions are presented in Sec. 7.

II. DESIGN AND SPECIFICATIONS OF THE HIP EXOSKELETON

2.1 Design of the hip exoskeleton

The proposed hip exoskeleton is illustrated in Fig. 1, comprising seven major components: a back brace, a back frame, a battery module, two hip actuators, two thigh frames, and two thigh supports. The device is designed to be symmetric about the wearer's sagittal plane, ensuring

Tzy-Qian Pai and Shi-Mou Lin are with the Department of Mechanical Engineering, National Cheng Kung University, Tainan, Taiwan. Chao-Chieh Lan is with the Department of Mechanical Engineering, National Taiwan University, Taipei, Taiwan. (Corresponding author email: lancc@ntu.edu.tw).

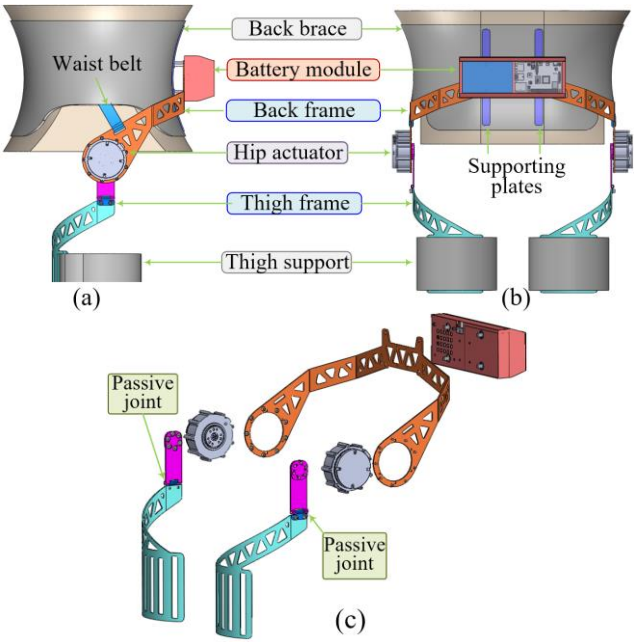

Fig. 1 Illustrations of the proposed hip exoskeleton (a) Side view (b) Back view (c) Exploded view

balanced force distribution during walking. The back frame serves as the central structural element, attached to the wearer via a back brace and two curved supporting plates that conform to the lumbar region. Onboard electronics and power are housed in a battery module mounted to the back frame, which contains a 3400-mAh Li-ion battery and a Raspberry Pi controller responsible for regulating actuator output torque.

Each hip actuator is a Xiaomi CyberGear quasi-direct drive unit with a gear ratio of 7.75, a weight of 317 g, and a maximum output torque of 12 Nm. The actuator output shaft connects to a thigh frame via a passive revolute joint, and each thigh frame is secured to the wearer's leg through a soft thigh support. This arrangement, summarized in the component connection diagram in Fig. 2, provides two active degrees of freedom for assisting hip flexion and extension in the sagittal plane during walking.

2.2 Passive joint placements

The hip exoskeleton has two passive revolute joints to improve comfort and adaptability. These joints serve two purposes: compensating for axial misalignment between the wearer's anatomical hip center and the actuator axis, and permitting natural leg abduction and adduction in the frontal plane. Without such compliance, misalignment would generate unintended forces on the wearer's thigh and back, causing discomfort during extended use. In Fig. 2, passive joints can be placed at three locations along the kinematic chain. The proposed design places the passive revolute joints between the hip actuator and the thigh frame, balancing actuator stability with adequate frontal plane mobility.

2.3 Single-piece back frame and thigh frame

In Fig. 1, both the back frame and thigh frame are constructed from stainless steel using laser cutting and sheet metal processing techniques, making them economically advantageous. Since the back frame can be readily bent to

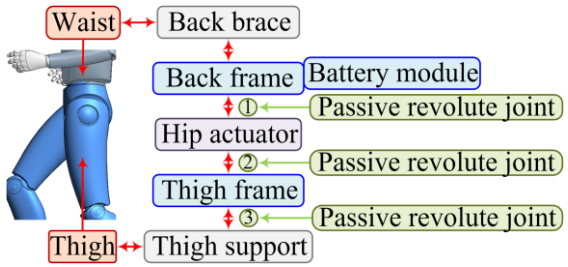

Fig. 2 Component connection diagram of the hip exoskeleton and possible locations of the passive revolute joint

conform to the natural curvature of the wearer's back, it can be precisely shaped to accommodate an individual's waist size without requiring additional adjusting mechanisms. Similarly, the thigh frame can be custom-manufactured to match the wearer's thigh size, again eliminating the need for adjusting mechanisms. Consequently, both frames can each be produced from a single piece of metal, resulting in lightweight and durable structures that reduce the total number of component parts and simplify the overall complexity of the exoskeleton.

A three-dimensional scanner may be employed to determine the shape and dimensions of an individual's waist and thigh, including waist size in both the frontal and sagittal planes, thigh length, and thigh circumference. Based on these measurements, the back and thigh frames can be fabricated to ensure a precise fit for each individual.

2.4 Specifications of the hip exoskeleton

Table 1 summarizes the specifications of the proposed hip exoskeleton. The total system mass is 2.1 kg, distributed among the hip actuators (28%), structural frames (51%), and battery module (21%). To determine the required actuator torque, we follow the guideline in [17], which recommends that assistive torque should be 20% of the wearer's maximum hip torque to effectively reduce metabolic cost. For a 75 kg wearer at a normal walking speed of 1.35 m/s, the maximum hip torque is approximately 60 Nm [12], yielding a target assistance torque of 12 Nm — precisely the rated output of the selected actuator. The torque-to-exoskeleton-mass ratio of the proposed device reaches 5.71 Nm/kg, and the maximum actuator angular velocity of 1776 °/s comfortably exceeds the maximum hip joint angular velocity during walking, which remains below 360 °/s.

Table 1 also includes three representative hip exoskeletons employing quasi-direct drive, cable-driven, and linear actuator technologies for comparison. While these designs vary in actuation approach, the proposed exoskeleton achieves a notably higher torque-to-mass ratio, demonstrating the effectiveness of the single-piece frame design and compact actuator selection in minimizing overall system weight.

2.5 Prototype of the hip exoskeleton and customized back and thigh braces

Fig. 3 shows a prototype of the hip exoskeleton worn by a participant with a weight of 65 kg and a height of 175 cm. The back and thigh frames were custom fabricated to match the participant's waist and thigh dimensions, measured using

Table 1 Specifications of the proposed hip exoskeleton and comparisons with existing designs

Specification	Ours	[5]	[10]	[12]
Total mass (kg)	2.1	3.4	3.6	7.0
Battery mass (kg)	0.257	0.548	0.372	1.04
Actuation type	Quasi-direct drive		Cable-driven	Linear actuator
Maximum output torque (Nm)	12	17.5	9	14.1
Torque-to-exoskeleton-mass ratio (Nm/kg)	5.71	5.15	2.50	2.01

Fig. 3 Prototype of the hip exoskeleton (a) Side view (b) Back view (c) Front view

a three-dimensional scanner as described in Sec. 2.3. The back frame was bent to conform closely to the natural curvature of the wearer's lumbar region, distributing the load evenly across the back and minimizing localized pressure. The thigh frames were similarly shaped to wrap around the wearer's thighs, and soft thigh supports were attached to improve contact comfort during prolonged use.

As Fig. 3(c) shows, the passive revolute joints allow the wearer to move their legs freely in the frontal plane, enabling natural abduction and adduction during walking. This is particularly important during turns or lateral weight shifts, where rigid fixation would otherwise cause discomfort or restrict natural movement. Compared to designs without passive joints, the proposed configuration reduces unintended constraint forces on the wearer's hip and thigh, improving overall wearability.

III. TORQUE CONTROL STRATEGY

3.1 Torque control strategy

For the hip exoskeleton to provide assistance rather than resistance during actual walking, the assistive torque profile of the hip actuator should be controlled to lead the gait cycle of the wearer. The Delayed Output Feedback Control (DOFC) strategy [18] is used in the paper to generate assistive torques. As shown in Figs. 4(a) and 4(b), the left and right hip joint angles are denoted as q_L and q_R, respectively. The joint angles can be obtained by the encoders of the hip actuators. A smoothing filter is applied to the raw angle measurements obtained from the encoder:

$$q^{cur} = (1-\alpha)q^{prv} + \alpha q^{cur}_{raw} \quad (1)$$

In this filtering step, q^{prv} represents the previously filtered joint angle, and q^{cur} represents the current raw measurement from the encoder. The filtering coefficient α (ranging from 0 to 1) adjusts the smoothness of the measured angle. A

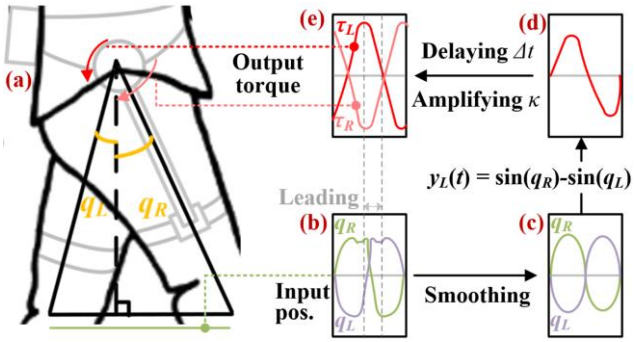

Fig. 4 (a-b) Left and right hip joint angles (c) Smoothing of the joint angles (d) Sinusoidal-like output function (e) Output torque

Fig. 5 Experimental setup of efficiency evaluation

smaller α value emphasizes past measurements, reducing high-frequency noise and creating smoother angles, thereby improving the stability of the torque output. After smoothing q_L and q_R as shown in Fig. 4(c), two sinusoidal-like output functions y_R and y_L are defined as follows:

$$y_R = \sin q_L - \sin q_R; y_L = \sin q_R - \sin q_L \quad (2)$$

In Fig. 4(d), the difference between these angles captures the symmetry and phase differences of the wearer's gait, converting angular displacement into a normalized sinusoidal signal ranging between −1 and 1. This sinusoidal form effectively captures gait periodicity, simplifying torque generation synchronized with the wearer's gait cycle. A controlled time delay Δt and a gain factor κ are introduced to generate leading assistive torques:

$$\tau_R = \kappa y_R(t-\Delta t); \tau_L = \kappa y_L(t-\Delta t) \quad (3)$$

In Eq. (3), the output torque commands for the right and left joints are delayed by a specific time interval Δt, as shown in Fig. 4(e). This intentional delay ensures the exoskeleton's torque leads rather than follows the wearer's movement, providing assistance proactively rather than reactively. The parameter κ is a scaling factor that adjusts torque amplitude to meet varying assistive needs for different walking speeds or terrain conditions.

3.2 Torque and angular rotation profiles

Fig. 5 shows the experimental setup to measure the joint torque and joint angle of the hip exoskeleton during actual walking. A wearer walks on a treadmill that is controlled at a speed of 5 km/h. Instead of using the battery module, an external power source was used for ease of power measurement. Based on the DOFC strategy in Sec. 3.1, the values of Δt and κ were tuned to be 0.4 s and 7.8,

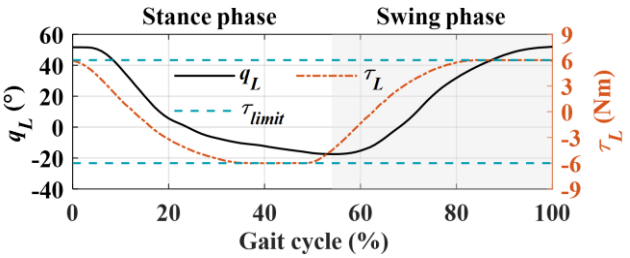

Fig. 6 Torque and angular rotation profiles

Table 2 Participant information and experienced optimal time delay

Number	Height (cm)	Weight (kg)	Age (yr)	Optimal Δt (s)
1	179	75	25	0.4
2	176	70	23	0.35
3	179	64	25	0.35

respectively. Fig. 6 shows the experimental torque and angle profiles of the left hip joint with respect to the gait cycle, respectively. The grey area indicates positive angular velocity and hence the swing phase. The white area indicates negative angular velocity and hence the stance phase. The swing phase occupies 40% of the entire gait cycle. Because a torque limit of 6 Nm was given to the hip actuators, the torque profile was constrained to the range between 6 and −6 Nm. The torque profile leads the angle profile during both the swing phase and the stance phase.

IV. EVALUATION OF OPTIMAL ASSISTANCE BASED ON PARTICIPANTS' FEEDBACK

4.1 Participants' feedback

Three healthy male participants were involved in the evaluation experiment. Their basic characteristics are listed in Table 2. At the speed of 5 km/h, different values of time delay were tested for each participant. Fig. 7 shows normalized torque profiles of Participant #3's left hip with respect to gait cycle. As can be seen, each time delay exhibits a different torque profile. The participant experienced different assistance or resistance for each time delay. Based on each participant's feedback, the time delay that provided the most significant assistance was obtained and listed in Table 2. This time delay is denoted as the optimal time delay. Fig. 8 further shows the torque profiles generated using the optimal time delay for each participant. The torque profiles are very close, indicating that different participants share almost the same torque profile regardless of the time delay.

The results in Fig. 8 are valid for the walking speed of 5 km/h. The optimal time delay at different speeds was also investigated based on Participant #1's feedback. Table 3 shows the optimal time delay of Participant #1 at different walking speeds. The time delay increases as the walking speed decreases. Fig. 9 further shows normalized torque profiles of Participant #1 with respect to different walking speeds. Although different walking speeds result in different step lengths and optimal values of time delay, the torque profiles are almost identical. Hence, the optimal torque profile in Figs. 8 and 9 can be applied to different participants at different speeds.

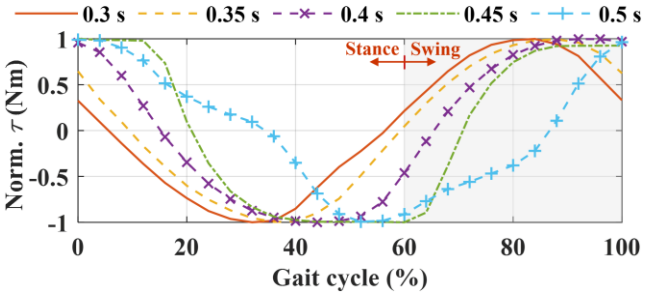

Fig. 7 Torque profiles for different values of time delay (Participant #3)

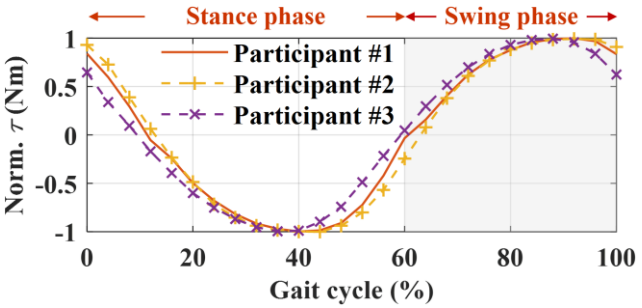

Fig. 8 Optimal torque profiles of different participants

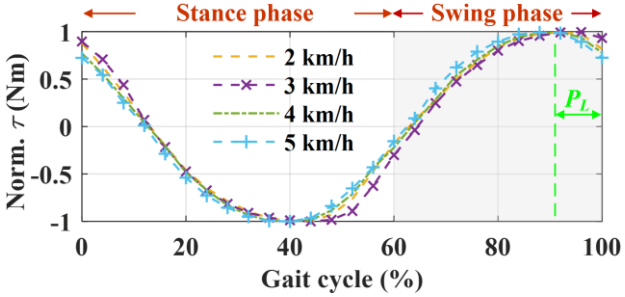

Fig. 9 Optimal torque profiles at different walking speeds (Participant #1)

Table 3 Optimal time delay of Participant #1 at different speeds

Walking speed (km/h)	2	3	4	5
Optimal Δt (s)	0.7	0.55	0.45	0.4

4.2 Generalization of torque profile

In Fig. 9, we denote the phase difference between the peak of the torque profiles and the end of the gait cycle as P_L. The value of P_L is nearly 10% of the gait cycle. The value of P_L can be used to determine the phase difference P_D between the y function and the torque profile as follows:

$$P_D = 44\% - P_L \tag{4}$$

where 44% is the phase difference between the peak of the y function and the end of the gait cycle. Given P_D, we can obtain the optimal time delay as follows:

$$\Delta t = T_g (P_D / 100\%) \tag{5}$$

where T_g is the period of each gait cycle. Based on the experimental results in Figs. 8-9, Eq. (5) can be used to determine the optimal time delay for different participants at various speeds.

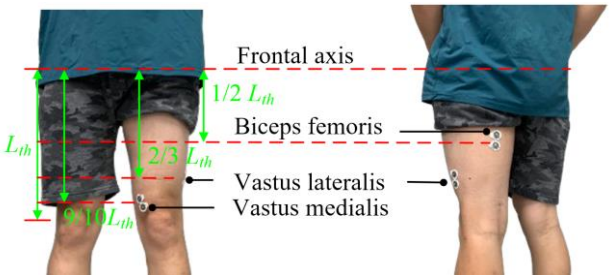

Fig. 10 Placement of the sEMG electrodes

V. SEMG-BASED EXPERIMENTAL VERIFICATION OF THE HIP EXOSKELETON PERFORMANCE

5.1 Surface electromyography experiment

To validate the proposed hip exoskeleton and evaluate the effect of optimal time delay obtained in Sec. 4 on the exoskeleton assistance magnitude, an experimental verification based on surface electromyography (sEMG) was conducted. Surface EMG signals provide direct measurements of muscle activation, offering an effective means to quantitatively assess how much the hip exoskeleton reduces the muscular effort during movement. In particular, sEMG signals reflect the neural activation levels of muscle groups involved in walking, serving as valuable indicators of the assistive performance and comfort provided by wearable robotic systems.

In the experiment, sEMG signals were collected from muscles involved in walking, including the vastus medialis (VM), vastus lateralis (VL), and biceps femoris (BF). The selection of these muscles was motivated by their significant roles in gait cycles—particularly their contributions to hip joint control. To ensure repeatability and accuracy, sEMG electrode patches (Covidien, H124SG) were placed according to standardized guidelines [19]. Fig. 10 shows the placements of electrode patches on different muscles of Participant #1's left thigh, with positions determined relative to the thigh length of the participant. Participant #1 has a thigh length of 46 cm.

Before conducting the exoskeleton assistance experiment, baseline sEMG measurements were established with the participant seated and relaxed, ensuring accurate and consistent comparisons between assisted and unassisted conditions. All sEMG signals were filtered between 20 and 500 Hz, amplified, and finally rectified to remove artifacts and noise. Experiments were performed on the treadmill shown in Fig. 5 at a fixed speed of 5 km/h. To compare with the results in Sec. 4, the delayed output feedback control method was again used.

Fig. 11 shows the vastus medialis sEMG activity with and without the exoskeleton assistance. For each curve in Fig. 11, 20 repeated gait cycles were performed to obtain the averaged sEMG signal and error band, which are shown as the solid line and shaded region, respectively. For the curve with exoskeleton assistance, a time delay of Δt = 0.4 s was used. The sEMG signal has a maximum amplitude of 0.25 V occurring in the stance phase. For the curve without the exoskeleton assistance, the participant still puts on the exoskeleton, but the motor power is off to allow full backdrivability. The sEMG signal can reach up to 1.00 V in

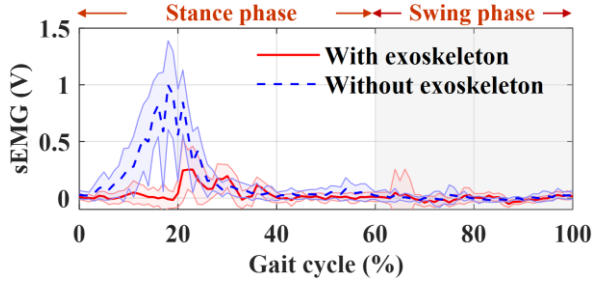

Fig. 11 Vastus medialis sEMG activity with and without exoskeleton assistance (Δt = 0.4 s)

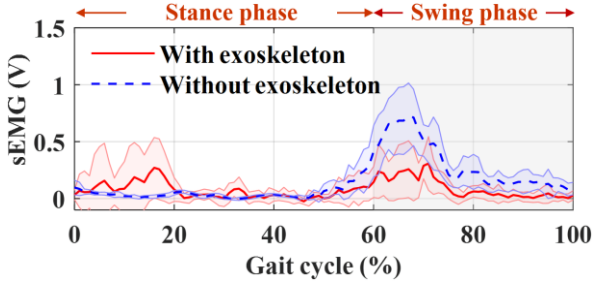

Fig. 12 Vastus lateralis sEMG activity with and without exoskeleton assistance (Δt = 0.4 s)

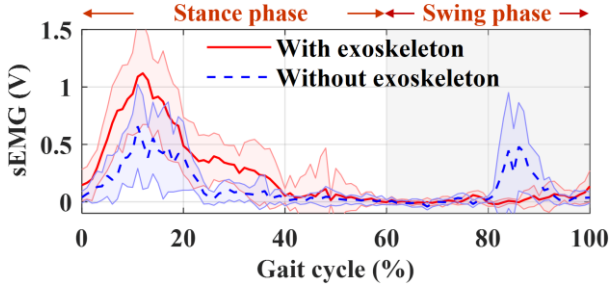

Fig. 13 Biceps femoris sEMG activity with and without exoskeleton assistance (Δt = 0.4 s)

the stance phase. Since the reduction of the sEMG signal is significant when comparing the two curves in Fig. 11, the exoskeleton robot can be shown to provide assistance effectively. Fig. 12 further shows the vastus lateralis sEMG activity with and without the exoskeleton assistance. The maximum sEMG voltage reduces from 0.72 V (without assistance) to 0.31 V (with assistance) in the swing phase. Both Figs. 11 and 12 show that the human muscle effort can be reduced by wearing the proposed hip exoskeleton with a proper time delay.

Fig. 13 further shows the biceps femoris sEMG activity with and without the exoskeleton assistance. The sEMG voltage is significantly reduced in the swing phase when exoskeleton assistance is provided. By contrast, the sEMG voltage slightly increases in the stance phase with exoskeleton assistance. At the time delay of Δt = 0.4 s, the effort of the biceps femoris is not obviously reduced when compared with vastus medialis or vastus lateralis.

5.2 Assistance ratio analysis

To quantify the assistance level of using the hip exoskeleton based on the sEMG signal, an assistance ratio is defined as follows:

$$A_g = \Sigma V_{ga} / \Sigma V_{gw} \tag{6}$$

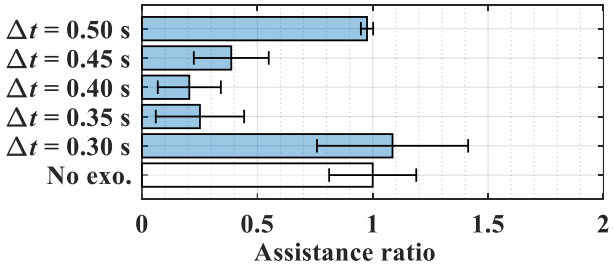

Fig. 14 Effect of time delay on the vastus medialis sEMG assistance ratio

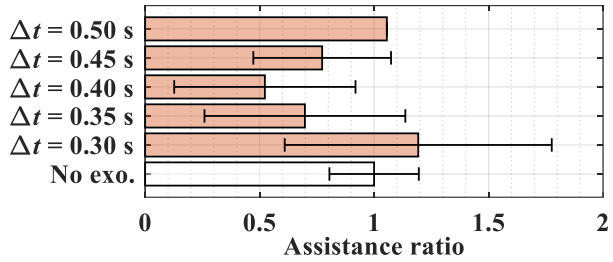

Fig. 15 Effect of time delay on the vastus lateralis sEMG assistance ratio

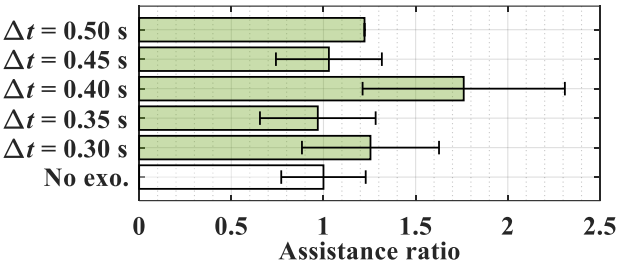

Fig. 16 Effect of time delay on the biceps femoris sEMG assistance ratio

where ΣV_{ga} and ΣV_{gw} represent the total sEMG voltage signal over a complete gait cycle with and without the exoskeleton assistance, respectively. An assistance ratio of less than one indicates that muscle activity is reduced and thus shows assistance. An assistance ratio of higher than one indicates that muscle activity is increased and thus shows extra human effort. Using the definition in Eq. (6), the assistance ratios are 0.20, 0.52, and 1.76 in Figs. 11, 12, and 13, respectively.

A range of time delay (Δt) from 0.3 to 0.5 s was evaluated in the sEMG experiment to determine the optimal value for comfort and muscular assistance. Fig. 14 shows the assistance ratios of the vastus medialis considering various values of time delay. As can be seen, a shorter or longer time delay results in a larger assistance ratio. The optimal time delay is 0.40 s, corresponding to the smallest assistance ratio and greatest overall reduction in muscular activation.

Fig. 15 further shows the assistance ratios of the vastus lateralis considering various values of time delay. Similarly, a shorter or longer time delay tends to increase muscle activity. The optimal time delay is also 0.4 s. Hence, at the delay setting of 0.4 s, the vastus medialis and lateralis muscles exhibited the most substantial decrease in muscle activation (approximately 35–45%). The results in Figs. 14-15 are consistent with the findings in Sec. 4 that the time delay of 0.4 s can give Participant #1 the optimal assistance

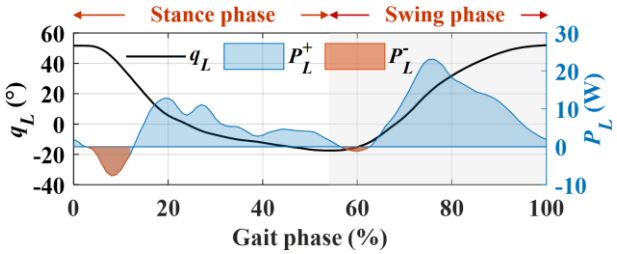

Fig. 17 Power of the left hip actuator

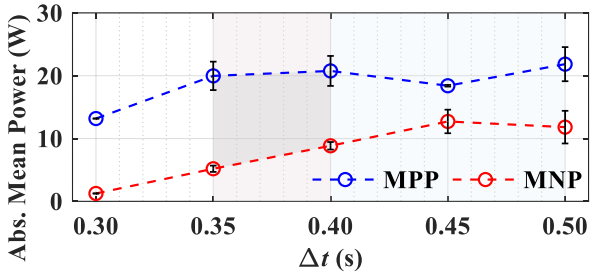

Fig. 18 Effect of time delay on the mean positive power and mean negative power

at the walking speed of 5 km/h. Hence, the sEMG measurements agree with the feedback from the participants. Eq. (5) can then be used to determine the optimal time delay without further sEMG measurements.

Fig. 16 shows the assistance ratios of the biceps femoris considering various values of time delay. The ratios are generally higher than one, indicating no decrease in muscle activation. At the delay setting of 0.4 s, the assistance ratio is the highest. Hence, the proposed exoskeleton might not optimally assist all muscle groups simultaneously. Overall, the sEMG experimental results demonstrated that the hip exoskeleton, combined with the optimized time delay, effectively reduced the average muscular effort and provided beneficial assistance during walking.

VI. EXPERIMENTAL POWER ANALYSIS OF THE HIP EXOSKELETON

During the sEMG experiments in Figs. 14-16, the power delivered from each actuator to the wearer's hip joint was also recorded. Fig. 17 shows the power of the left hip actuator in one gait cycle. The area of positive power is denoted as P_L^+, which indicates that the hip actuator torque is in the same direction as the angular velocity of the wearer's hip joint. Both the swing and stance phases show significant positive power, indicating that the hip exoskeleton is providing assistance. Two small areas of negative power, denoted as P_L^-, occur near the phase transition region. The negative power indicates that the hip actuator torque is in the opposite direction as the angular velocity of the wearer's hip joint, which should be minimized to avoid resistance to the wearer and, thus, energy loss. The negative power can be further reduced by adjusting the time delay Δt. In Fig. 17, the average value of the positive power is 10.3 W. Assuming that the motion profiles of the left and right hip joints are identical, the total positive power delivered to the wearer is 20.5 W.

Power curves similar to those in Fig. 17 were recorded to study the effect of time delay on the magnitude of the total

positive and negative power. Fig. 18 shows the mean positive power (MPP) and mean negative power (MNP) of each time delay. For clarity of comparison, the MNP curve was made non-negative by taking absolute values. The MPP curve reaches nearly 20 W after Δt = 0.35 s. By contrast, the MNP curve increases with the value of time delay, indicating more resistance to the participant. The MNP value should be kept small, and the MPP value should be kept large in order to increase the assistance level of the exoskeleton. In Fig. 18, the gray area between Δt = 0.35 s and 0.40 s meets such a requirement. Hence, the time delay between Δt = 0.35 s and 0.40 s can provide optimal assistance from power usage point of view. This is consistent with the result obtained from the sEMG experiments, where the time delay of Δt = 0.35 s to 0.40 s shows significant muscle activity reduction. Since sEMG electrodes may not be conveniently attached to a wearer's thigh during daily assistance, the actuator power profile can be used instead to evaluate the assistance level to the wearer.

VII. CONCLUSIONS

A lightweight hip exoskeleton was developed to provide efficient and adaptive walking assistance. The design integrates quasi-direct drive actuators, single-piece frames, and passive joints, achieving a high torque-to-mass ratio of 5.71 Nm/kg while maintaining comfort and structural reliability. A delayed output feedback control strategy was implemented, and user evaluations identified an optimal phase difference of approximately 10% between the torque profile and the end of the gait cycle. This phase-based strategy was shown to be consistent across different participants and walking speeds, enabling generalized assistance without the need for repeated calibration. Experimental results demonstrated that this strategy significantly reduced muscle activation in the vastus medialis and lateralis, consistent with subjective feedback, while power analysis confirmed increased positive power transfer with minimal resistive effects. These findings highlight the exoskeleton's capability to deliver physiologically meaningful and energetically efficient assistance, supporting its potential for mobility enhancement in everyday use.

REFERENCES

[1] Y.-Y. Su, Y.-L. Yu, C.-H. Lin, and C.-C. Lan, "A compact wrist rehabilitation robot with accurate force/stiffness control and misalignment adaptation," Int. J. Intell. Robot. Appl., vol. 3, no. 1, pp. 45–58, 2019.

[2] K.-Y. Wu, Y.-Y. Su, Y.-L. Yu, C.-H. Lin, and C.-C. Lan, "A 5-degrees-of-freedom lightweight elbow-wrist exoskeleton for forearm fine-motion rehabilitation," IEEE/ASME Trans. Mechatronics, vol. 24, no. 6, pp. 2684–2695, 2019.

[3] K.-Y. Wu, Y.-Y. Su, Y.-L. Yu, K.-Y. Lin, and C.-C. Lan, "Series elastic actuation of an elbow rehabilitation exoskeleton with axis misalignment adaptation," in Proc. IEEE Int. Conf. Rehabil. Robot. (ICORR), London, UK, 2017, pp. 567–572.

[4] H.-C. Hsieh, D.-F. Chen, L. Chien, and C.-C. Lan, "Mechanical design of a gravity-balancing wearable exoskeleton for the motion enhancement of human upper limb," in Proc. IEEE Int. Conf. Robot. Autom. (ICRA), Seattle, WA, USA, 2015, pp. 4992–4997.

[5] S. Yu, T.-H. Huang, X. Yang, C. Jiao, J. Yang, Y. Chen, J. Yi, and H. Su, "Quasi-direct drive actuation for a lightweight hip exoskeleton with high backdrivability and high bandwidth," IEEE/ASME Trans. Mechatronics, vol. 25, no. 4, pp. 1794–1802, 2020.

[6] A. Bajpai, C. Carrasquillo, J. Carlson, J. Park, D. Iyengar, K. Herrin, A. J. Young, and A. Mazumdar, "Design and validation of a versatile high torque quasi-direct drive hip exoskeleton," IEEE/ASME Trans. Mechatronics, vol. 29, no. 1, pp. 789–797, 2023.

[7] T. Zhang, M. Tran, and H. Huang, "Design and experimental verification of hip exoskeleton with balance capacities for walking assistance," IEEE/ASME Trans. Mechatronics, vol. 23, no. 1, pp. 274–285, 2018.

[8] Y. Qian, S. Han, Y. Wang, H. Yu, and C. Fu, "Toward improving actuation transparency and safety of a hip exoskeleton with a novel nonlinear series elastic actuator," IEEE/ASME Trans. Mechatronics, vol. 28, no. 1, pp. 417–428, 2022.

[9] I. Kang, R. R. Peterson, K. R. Herrin, A. Mazumdar, and A. J. Young, "Design and validation of a torque-controllable series elastic actuator-based hip exoskeleton for dynamic locomotion," J. Mech. Robot., vol. 15, no. 2, p. 021007, 2023.

[10] E. Tricomi, M. Mossini, F. Missiroli, N. Lotti, X. Zhang, M. Xiloyannis, L. Roveda, and L. Masia, "Environment-based assistance modulation for a hip exosuit via computer vision," IEEE Robot. Autom. Lett., vol. 8, no. 5, pp. 2550–2557, 2023.

[11] Y. H. Chang, J. S. Kang, B. R. Jeong, B. M. Lim, B. J. Choi, and Y. B. Lee, "Verification of walking efficiency of wearable hip assist robot for industrial workers: A preliminary study," J. Korean Soc. Precis. Eng., vol. 41, no. 1, pp. 37–46, 2024.

[12] I. Kang, H. Hsu, and A. J. Young, "Design and validation of a torque controllable hip exoskeleton for walking assistance," in Proc. ASME Dyn. Syst. Control Conf., Atlanta, GA, USA, 2018, vol. 51890, p. V001T12A002.

[13] M. K. Ishmael, D. Archangeli, and T. Lenzi, "A powered hip exoskeleton with high torque density for walking, running, and stair ascent," IEEE/ASME Trans. Mechatronics, vol. 27, no. 6, pp. 4561–4572, 2022.

[14] Y. Ma, D. Liu, Z. Yan, L. Yu, L. Gui, and C. Yang, "Optimizing exoskeleton assistance: Muscle synergy-based actuation for personalized hip exoskeleton control," Actuators, vol. 13, no. 2, p. 54, Jan. 2024.

[15] X. Zhang, X. Chen, B. Huo, C. Liu, X. Zhu, Y. Zu, X. Wang, X. Chen, and Q. Sun, "An integrated evaluation approach of wearable lower limb exoskeletons for human performance augmentation," Sci. Rep., vol. 13, no. 1, p. 4251, 2023.

[16] S.-M. Lin and C.-C. Lan, "Design and analysis of a lightweight hip exoskeleton robot," in Proc. Int. Symp. Mech. Transmissions Appl. (MeTrApp), 2025, vol. 192, pp. 104–114.

[17] I. Kang, H. Hsu, and A. Young, "The effect of hip assistance levels on human energetic cost using robotic hip exoskeletons," IEEE Robot. Autom. Lett., vol. 4, no. 2, pp. 430–437, 2019.

[18] B. Lim, J. Lee, J. Jang, K. Kim, Y. J. Park, K. Seo, and Y. Shim, "Delayed output feedback control for gait assistance with a robotic hip exoskeleton," IEEE Trans. Robot., vol. 35, no. 4, pp. 1055–1062, 2019.

[19] P. Konrad, "The ABC of EMG: A practical introduction to kinesiological electromyography," Noraxon USA, Scottsdale, AZ, USA, vol. 1, pp. 30–35, 2005.